

Emergence of chaotic behaviour in linearly stable systems

F. Ginelli^{*}, R. Livi[†] and A. Politi[‡]

November 9, 2018

Abstract

Strong nonlinear effects combined with diffusive coupling may give rise to unpredictable evolution in spatially extended deterministic dynamical systems even in the presence of a fully negative spectrum of Lyapunov exponents. This regime, denoted as “stable chaos”, has been so far mainly characterized by numerical studies. In this manuscript we investigate the mechanisms that are at the basis of this form of unpredictable evolution generated by a nonlinear information flow through the boundaries. In order to clarify how linear stability can coexist with nonlinear instability, we construct a suitable stochastic model. In the absence of spatial coupling, the model does not reveal the existence of any self-sustained chaotic phase. Nevertheless, already this simple regime reveals peculiar differences between the behaviour of finite-size and that of infinitesimal perturbations. A mean-field analysis of the truly spatially extended case clarifies that the onset of chaotic behaviour can be traced back to the diffusion process that tends to shift the growth rate of finite perturbations from the quenched to the annealed average. The possible characterization of the transition as the onset of directed percolation is also briefly discussed as well as the connections with a synchronization transition.

PACS numbers: 05.45+b

^{*}Dipartimento di Fisica, Università di Firenze and Istituto Nazionale di Fisica della Materia, Unità di Firenze

[†]Dipartimento di Fisica, Università di Firenze and Istituto Nazionale di Fisica della Materia, Unità di Firenze

[‡]Istituto Nazionale di Ottica Applicata and Istituto Nazionale di Fisica della Materia, Unità di Firenze

1 Introduction

Unpredictable evolution in dynamical systems is due to the propagation of information. For instance, the sensitivity of trajectories to infinitesimal perturbations implies that any arbitrarily small inaccuracy in the determination of the initial conditions is exponentially amplified in time, with an average rate associated to the positive component of the Lyapunov spectrum. The integral of this component, the so-called Kolmogorov-Sinai entropy [1], measures the production rate of information that flows from the less significant digits of the dynamical variables to the more significant ones. In particular, the existence of at least one positive Lyapunov exponent is a sufficient condition for identifying chaotic dynamics; conversely, a fully negative spectrum is suggestive of a periodic evolution.

This approach to unpredictable evolution based on linear stability analysis has been developed in the context of finite (low-dimensional) systems. Its extension to spatially extended dynamical systems is based on the implicit assumption that they can be viewed as a collection of almost independent, finite dimensional subsystems. The existence of a limit Lyapunov spectrum [2, 3] provides strong support to this hypothesis and typical chaoticity indicators, like entropies and generalized dimensions, can be turned into their corresponding densities [4]. In fact, a primary interest in the study of space-time chaos is the identification of thermodynamic-like properties.

However, Lyapunov instability is not the only source of unpredictability in such systems. Actually, information can also flow through the boundaries and be transmitted in space by nonlinear mechanisms of front propagation. The so-called chaotic rules of Deterministic Cellular Automata (DCA) [5] are typical examples of unpredictable evolution in the absence of linear instabilities. There, the discreteness of the state variable prevents the very existence of infinitesimal perturbation, while, on the other hand, even isolated “state-flips” may propagate through the lattice with finite velocity, giving rise to an irregular dynamics. In fact, any DCA rule defined over a lattice of L cells is bounded to exhibit a periodic behaviour, since the number of possible states is finite (b^L if b is the number of possible states in each given site). What makes a “chaotic” DCA rule different from an ordered one is the exponential growth of the recurrence time of the typical configurations. Accordingly, the unpredictable behaviour is dynamically persistent only in the infinite-size limit.

A very similar unpredictable behaviour, denoted as *stable chaos*, has been observed also in coupled map lattice (CML) models [6, 7] of the type

$$x_i(t+1) = f\left(\frac{\varepsilon}{2}x_{i-1}(t) + (1-\varepsilon)x_i(t) + \frac{\varepsilon}{2}x_{i+1}(t)\right) \quad , \quad (1)$$

where $x_i(t)$ is the continuous state variable at time t on the site i of a 1d lattice; the function f is a linearly stable map of the interval $[0, 1]$ into itself and ε is the strength of the diffusive coupling. It is worth pointing out that

this spatial coupling cannot produce any linear instability mechanism and the whole spectrum of Lyapunov exponents is found to be negative. Accordingly, the CML dynamics must eventually approach a periodic stable attractor. This notwithstanding, if f is equipped with a sufficiently strong nonlinearity (e.g. a discontinuity or a region with rapidly varying slope), one can find a region in parameter space, where the “transient” evolution towards the periodic attractor grows exponentially with the system size L , analogously to chaotic DCA rules. Despite there is no rigorous proof of this statement, many independent numerical studies confirm such a scenario (see, e.g., [8, 7]). Striking features of this “transient” regime are its stationarity and apparent ergodicity: for instance, space and time correlation functions decay exponentially like in usual chaotic phases, while ensemble averages coincide with time averages (provided that a size-independent pre-transient is discarded). Moreover, the maximum Lyapunov exponent is found to approach a stationary negative value, before quite suddenly turning to the value corresponding to the eventual attractor. Because of its exponential growth, the “transient” represent the truly relevant regime in the thermodynamic limit, while the periodic attractor(s) have no practical significance.

A careful inspection indicates that the mechanism of information production in stable chaos is a flow from the outer (left and right) parts of the chain, like in chaotic DCA rules [7]. Accordingly, the unpredictability of stable chaos relies on a genuine nonlinear propagation mechanism,

As we recall in section II, stable chaotic evolution can be detected by measuring *damage spreading*, i.e. the average velocity of a front propagating into an unperturbed region. This indicator can be viewed as a sort of generalization of the standard Lyapunov exponent and the use of a proper metric, attributing an increasingly smaller weight to the farther sites would make the correspondence more transparent[7]. However, it is worth noting that the front velocity does not allow defining an analogous of a negative Lyapunov exponent, since in the ordered phase a perturbation does not only regress but also decreases everywhere in size leading to the disappearance of the front itself.

Numerical studies of stable chaos have contributed to shed some light on the relationship between this dynamical regime and the appearance of many interesting complex phenomena, such as nonequilibrium phase transitions, spiral chaos, and the propagation of rough interfaces [9, 10, 11]. However, little is rigorously known about the underlying mechanisms. The aim of this paper is precisely to make some progress in this direction by investigating the conditions under which finite perturbations can propagate instead of die out. In analogy to various analytical techniques introduced to estimate the maximum Lyapunov exponent in standard chaotic CMLs [12, 13], here we assume that the evolution in phase-space generates a truly random pattern, characterized by short range correlations and thereby introduce a suitable stochastic model describing the evolution in the difference space. Besides diffusion, the model dynamics allows for a random alternancy of a contraction and an expansion process the proba-

bility of which depends on the perturbation size. First of all, in Sec. II we verify that, with an appropriate choice of the parameter values, the model is able to reproduce not only qualitatively but also quantitatively the main features of stable chaos. Afterwards, we further simplify the rule determining the expansion process to reduce the subsequent technicalities, while keeping untouched the key ingredients of the model.

In order to understand how a finite perturbation can be sustained even in the presence of an average contraction rate, in Sec. III we first discuss the uncoupled, i.e. 0-dimensional, case, where, by definition, propagation of perturbations is absent. The negative Lyapunov exponent obviously implies that perturbations are eventually absorbed, so that stable chaos cannot exist in this framework. Nonetheless, the presence of a non-uniform contraction process yields nontrivial properties of the dynamics. They are exemplified by the difference existing between the standard multifractal spectrum (associated to infinitesimal perturbations) and the spectrum defined in this paper to describe the evolution of finite perturbations. In fact, a noteworthy result of Sec. III is that it is possible to define a finite-size multifractal spectrum independently of the initial amplitude of the perturbation. Finally, in Section III we comment about the connection with the finite-size Lyapunov exponents recently proposed by some authors as a tool to characterize dynamical unpredictability, beyond standard linear stability analysis [14, 15].

The methods and concepts introduced in Section III are applied in Section IV to the study of the spatially extended version of the stochastic model. For the sake of space, we limit our discussion to the case of “democratic” coupling, but it is clear that stable chaos arises in a broad region of strong coupling. It is precisely the diffusive coupling to be responsible for the sustainment of stable chaos. Over small scales, contraction is more effective than the sporadic amplification: in such circumstances, diffusion just levels the damping process. Conversely, at larger scales, diffusion proves to be an effective mechanism to propagate locally generated amplifications. The net effect is that, in suitable parameter regions, perturbations self-sustain.

By introducing a factorization hypothesis of the spatial degrees of freedom, we obtain a good estimate of the probability distribution associated with the spatially extended dynamics. In particular, we find a critical value of the contraction rate separating a dynamical regime, where any perturbation eventually vanishes, from a truly chaotic phase, where the average value of the perturbation remains finite in the infinite-time limit. A mean field argument provides a suggestive description of this scenario: the diffusive coupling induces a shift of the finite-size Lyapunov exponent that grows from the negative quenched average (corresponding to the uncoupled limit) towards the annealed average of the expansion rate. Depending on the parameter values, this latter average may be strictly larger than 0, thus implying that the zero-amplitude regime is unstable.

The transition exhibited by the stochastic model is reminiscent of the “fuzzy”

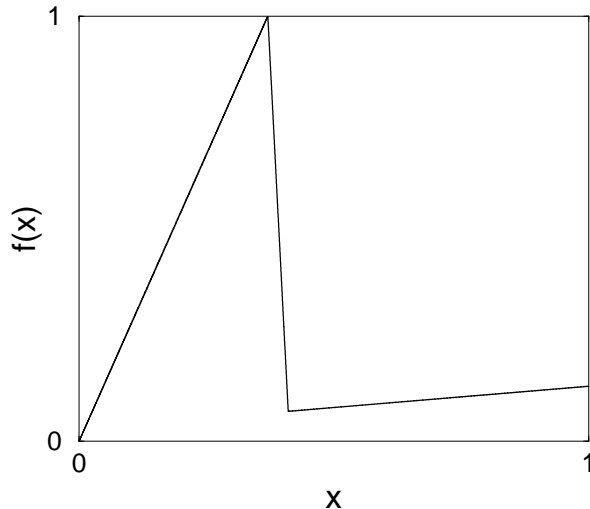


Figure 1: Picture of the local deterministic map (2) for typical parameter values.

transition region found in a deterministic CML [17]. However, we cannot push the analogy to a quantitative level, since the stochastic CML dynamics is self-generated and thus it is increasingly regular while approaching the transition region (this is the main reason for the fuzziness observed in Ref. [17]), while here the stochastic properties of the contraction/expansion process is fixed a priori. A tight analogy, instead, exists with the stochastic synchronization induced by an additive noise [18]. Indeed, in this context, the external noise does not change its robust stochastic features when passing from the synchronized to non-synchronized regime. It is precisely this analogy which suggests that the transition described in this paper should belong to the universality class of directed percolation [19]. The numerical simulations described in Sec. V do confirm such an expectation, but subtle problems still prevent us from still drawing definite conclusions. Such open problems and the possible future perspectives are summarized in Sec. V.

2 Generalities

The typical functions used to investigate stable chaos in CML are piecewise linear maps of the unit interval of the form (see also Fig. (1) for a pictorial

representation)

$$f(x) = \begin{cases} c_1 x & 0 \leq x < 1/c_1 \\ 1 - (x - 1/c_1)(1 - c_2)/\Delta & 1/c_1 \leq x < 1/c_1 + \Delta \\ c_2 + c_3[x - (1/c_1 + \Delta)] & 1/c_1 + \Delta \leq x \leq 1 \end{cases} . \quad (2)$$

The most studied case in the literature [7] corresponds to the limit $\Delta \rightarrow 0$, where $f(x)$ reduces to a discontinuous function. As we shall comment along this paper, a strong nonlinear component of map $f(x)$, rather than a true discontinuity, is sufficient to yield stable chaos. This is why we prefer to consider here the more general case (2). The parameter range of interest for the present study is when all initial conditions (except for a set of zero Lebesgue measure) converge to the same periodic orbit. For instance, for $c_1 = 2.7$, $c_2 = 0.07$, $c_3 = 0.1$ and $\Delta = 0.01$, a stable period-3 orbit exists with Lyapunov exponent $\lambda = -0.316\dots$ As already mentioned in the Introduction, there is a range of values of the diffusive coupling ε defined in (1), where the CML dynamics exhibits a “chaotic” evolution, despite the largest Lyapunov exponent is negative. Damage spreading analysis provides a first hint about this mechanism, that is responsible for the sustainment of irregular behaviour. More precisely, while standard chaos amounts to a flow of information from the less to the more significant digits, stable chaos is generated by a flow of information from the outer (left and right) to the inner parts of an infinite chain. Unfortunately, while the former flow can be “easily” studied thanks to the linearity of the process (in fact, over sufficiently small scales, any smooth function can be linearized), the same argument does not apply to the dynamics on the left and right edges, that is equally nonlinear at any spatial position.

This is the main reason for the difficulty in deriving the necessary and sufficient conditions for the propagation of perturbations. Moreover, while the dynamics of an infinitesimal perturbation can be studied by neglecting propagation phenomena, the opposite is not possible. One cannot study propagation without properly accounting for the local contraction/expansion mechanisms.

The damage spreading analysis is performed by studying the dynamical variable $u_i(t) = |x_i(t) - y_i(t)|$, i.e. the absolute value of the difference between two test trajectories, $x_i(t)$ and $y_i(t)$, that are initially set equal to one another on the right of some lattice site, say $i = 0$, while they are assumed to be totally independent on the left. With such a setting, the damage spreading analysis amounts to studying the propagation of a front separating the region in space where $u_i(t) \sim \mathcal{O}(1)$ (the tail) from the region where the two trajectories converge to each other, $u_i(t) \sim 0$ (the forefront).

The first conceptual problem that we have to face is not just the propagation of the front, but its self-sustainment in spite of the local average contraction rate. In order to shed some light on this crucial point, we have simplified the model by assuming that the dynamics is indeed irregular, thereby determining whether this assumption is consistent with the sustainment of an $\mathcal{O}(1)$ perturbation.

This is analogous to the consistency approach developed for the description of standard chaos, where complete randomness of the multipliers of the evolution operator in the “difference” space is assumed in order to estimate the maximum Lyapunov exponent [12, 13].

Accordingly, we introduce a suitable stochastic model to describe the evolution in the “difference” space spanned by $u_i(t)$. Let us start from the simple case $\Delta = 0$. With reference to the CML dynamics, the dynamical rule is composed of two steps. The first one corresponds to the application of the standard discrete diffusive operator

$$\tilde{u}_i(t) = (1 - \varepsilon)u_i(t) + \frac{\varepsilon}{2}u_{i+1}(t) + \frac{\varepsilon}{2}u_{i-1}(t) \quad , \quad (3)$$

where $0 \leq \varepsilon \leq 1$ is the coupling parameter. The second step contains the stochastic component of the evolution rule,

$$u_i(t+1) = \begin{cases} r_i(\tilde{u}_i, t), & \text{w.p. } p = \min[1, b\tilde{u}_i(t)] \\ a\tilde{u}_i(t), & \text{w.p. } 1 - p \end{cases} \quad , \quad (4)$$

where, “w.p.” is the shorthand notation for “with probability”, while $r_i(\tilde{u}_i, t)$ is a random number distributed in the unit interval according to some probability distribution that depends on \tilde{u}_i .

This is the non-trivial part of the stochastic model, defined to mimick the evolution of perturbation in the CML dynamics. The first line describes the instability mechanism associated with the discontinuity while the second line describes the contraction of $u_i(t)$ by a constant factor ¹ $0 < a < 1$. In the CML model, the instability mechanism arises whenever the test trajectories, $x_i(t)$ and $y_i(t)$, lie on different sides of the discontinuity of the map. In this case, the value taken by the difference variable $u_i(t+1)$ is not uniquely determined by the value of $u_i(t)$, since it depends also on $x_i(t)$. In particular, for small values of $u_i(t)$, the instability mechanism occurs quite rarely (it is unlike that the discontinuity is placed across two nearby trajectories) and $u_i(t+1)$ is amplified by a big factor; conversely, for large values of $u_i(t)$, the discontinuity plays a role much more frequently, but it is less effective. The numerical analysis of the CML model shows that the probability p of the instability mechanism grows linearly for small values of the difference variable $u_i(t)$ and approaches 1 when $u_i(t)$ does the same. Accordingly, in the stochastic model (4), we have decided to schematize this dependence with the simple law $p = \min[1, b\tilde{u}_i(t)]$.

Such a stochastic model can be straightforwardly generalized to cover the case corresponding to a CML dynamics with a nonzero Δ . The main difference is that, whenever \tilde{u} is smaller than Δ , u is expanded by a fixed factor Δ^{-1} with a constant probability $b\Delta$, while the previous stochastic rule still applies for $\tilde{u} > \Delta$. This amounts to assuming that only perturbations larger than Δ

¹For the sake of simplicity we assume that the contraction rate is a constant, as in [6].

perceive the steep branch of the map as an effective discontinuity. Accordingly, Eq. (4) is replaced by

$$u_i(t+1) = \begin{cases} r_i(\tilde{u}_i, t), & \text{w.p. } p = \min[1, b\tilde{u}_i(t)] \\ a\tilde{u}_i(t), & \text{w.p. } 1-p \end{cases}, \quad \text{if } \tilde{u}_i(t) > \Delta, \\ u_i(t+1) = \begin{cases} \tilde{u}_i(t)/\Delta, & \text{w.p. } p = b\Delta \\ a\tilde{u}_i(t), & \text{w.p. } 1-p \end{cases} \quad \text{if } \tilde{u}_i(t) \leq \Delta. \quad (5)$$

One can easily check that these formulae reduce to Eq. (4) in the limit $\Delta \rightarrow 0$.

The maximum Lyapunov exponent of the CML dynamics corresponds to the time average of the expansion rates of infinitesimal perturbations. In the context of the stochastic model, it naturally corresponds to the quantity

$$\lambda_0 = \lim_{t \rightarrow \infty} \lim_{u(0) \rightarrow 0} \frac{1}{t} \sum_{\tau=0}^{t-1} \ln \frac{\|u_i(\tau+1)\|}{\|u_i(\tau)\|} = \lim_{t \rightarrow \infty} \lim_{u(0) \rightarrow 0} \frac{1}{t} \ln \frac{\|u_i(t)\|}{\|u_i(0)\|}, \quad (6)$$

that we still denote as the “maximum Lyapunov exponent”.

An analytical estimate of λ_0 can be obtained by a mean-field argument, according to which the probability of applying the expansion factor $1/\Delta$ is $b\Delta$, while the probability of applying the contraction factor a is $1 - b\Delta$. One easily obtains

$$\lambda_0 \approx b\Delta \ln\left(\frac{1}{\Delta}\right) + (1 - b\Delta) \ln a = \ln a - b\Delta \ln(a\Delta) \quad . \quad (7)$$

Numerical simulations indicate that the true value of λ_0 is generally slightly larger than this mean-field estimate.

Moreover, for $\Delta = 0$, $\lambda_0 \approx \ln a < 0$, while for increasing values of Δ it may become positive, indicating that a standard chaotic regime is attained². Here, we are interested in studying only the parameter region where λ_0 remains negative.

2.1 Comparison between stochastic and deterministic models

The reliability of the stochastic models (4) and (5) has been tested by numerical simulations which show that both rules (4) and (5) together with the diffusive coupling (3), exhibit the same qualitative features of the CML dynamics (1), (2). In particular, when the contraction is relatively strong, any initial perturbation $u_i(0)$ is quickly absorbed to the fixed point $u_i = 0 \quad \forall i$: this regime corresponds to the “ordered” or, equivalently, to the “synchronized” phase. On the other hand, for weaker contractions, almost any initial condition evolves towards an

²This is not entirely correct, since, as discussed in Ref. [20], the standard chaotic regime occurs when a stronger constraint is met: the linear propagation velocity coincides with the nonlinear one.

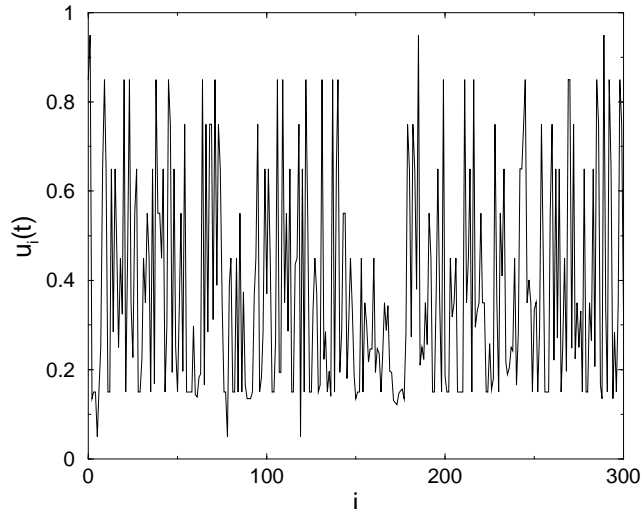


Figure 2: Snapshot of the perturbation profile in the chaotic phase of the stochastic model (3, 5) at time $t = 500$.

irregular spatial structure like the one shown in Fig. 2. In this case, the space average

$$\bar{u}(t) = \frac{1}{L} \sum_{i=1}^L u_i(t) \quad (8)$$

remains finite and $\bar{u}(t) = u^*$, independently of t and L for sufficiently large sizes. To be more precise, perturbations of the order $\mathcal{O}(1)$ survive only for a finite time τ also in the chaotic phase of the stochastic model. Nevertheless, in analogy to the CML model, τ grows exponentially with the lattice size L . Furthermore, ensemble averages indicate that this regime is asymptotically stationary in time and the comparison with time averages (obviously performed over times much shorter than τ) indicate that ergodicity holds as well. It is therefore meaningful to define the single-site probability distribution $Q(t, v)$ of finding a perturbation u_i in between v and $v + dv$ at time t , and its stationary limit $Q(v)$, attained for large enough times. It is also worth introducing the space and ensemble averages $m(t) = \langle \bar{u}(t) \rangle$ (from here on, unless otherwise stated, $\langle \cdot \rangle$ denotes an ensemble average) and the stationary limit, $m(t) \rightarrow \bar{m}$.

In the numerical investigations we have assumed no-flux boundary conditions as they preserve the $u = 0$ fixed point and are reasonably harmless in the chaotic phase. The \tilde{u} -dependent probability distribution of the random variable $r_i(\tilde{u}_i, t)$ has been reconstructed from the CML dynamics. Moreover, in order to avoid boundary effects in the damage spreading analysis, the lattice size has always been chosen in such a way that the perturbation front never reaches the lattice

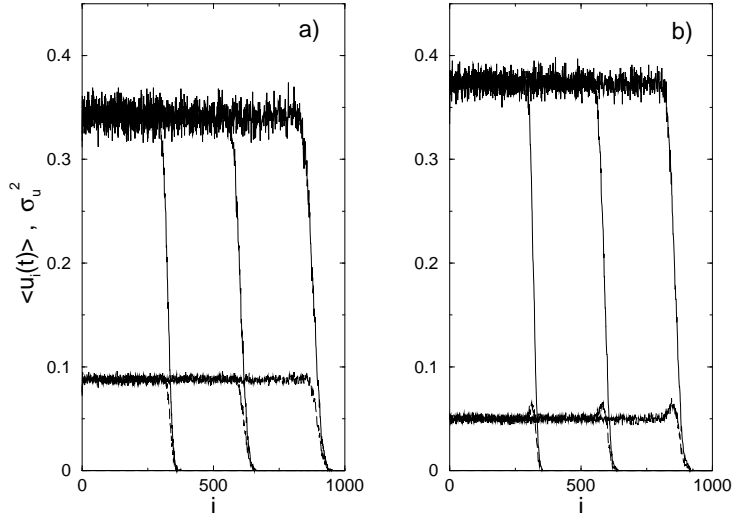


Figure 3: Average front profiles (upper curves) and the corresponding variances (lower curves) at three different times, $t = 500$, $t = 1000$ and $t = 1500$. Panel (a) refers to the deterministic CML model (1),(2), with parameter values $c_1 = 2.7$, $c_2 = 0.07$, $c_3 = 0.1$, $\Delta = 0$, $\varepsilon = 2/3$; averages have been performed over 10^3 initial conditions. Panel (b) refers to the stochastic model (3), (4), with parameter values $a = 0.9$, $b = 1.7$, $\Delta = 0$, $\varepsilon = 2/3$; averages have been performed over 10^3 realizations, while the probability distribution for $r_i(\bar{u}_i, t)$ and the values of parameters a and b have been determined from the CML model depicted in the left panel.

edges during each simulation.

In order to investigate damage spreading phenomena, the initial conditions have been fixed by imposing $u_i(0) = 0$ for $i > 0$ and randomly choosing $u_i(0)$ with a uniform probability distribution in the interval $[0, 1]$ for $i \leq 0$. The statistical fluctuations showed by $u_i(t)$ have been smoothed out by performing ensemble averages (over different realizations of the stochastic process) of the spatial configurations at equal times. In the chaotic phase, the initial “kink”-like structure persists: the front connecting the perturbed with the synchronized region moves with a fluctuating velocity. The ensemble averages corresponding to three different times are reported in Fig. 3b, where they are compared with the results directly obtained from the CML model (for the sake of space we limit ourselves to consider the case $\Delta = 0$ a), where ensemble averages are performed over different initial conditions. Several observations are in order. First, we notice that, in spite of the simplifications introduced in the stochastic model (besides the lack of space-time correlations, we have indeed assumed a constant contraction rate as if the two branches of the local map (2) had the same slope),

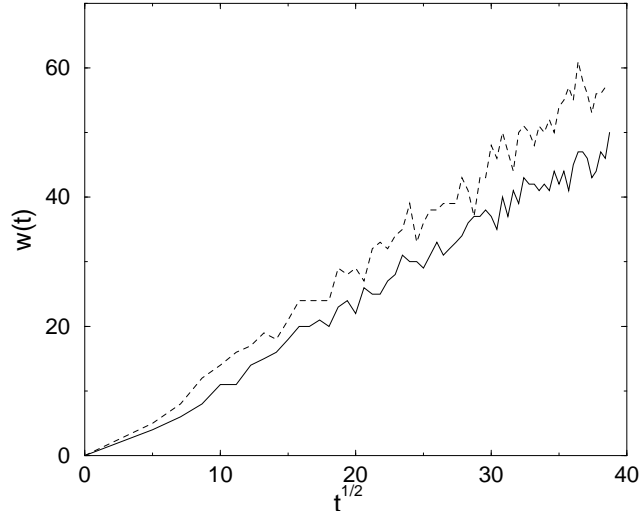


Figure 4: The average front size $w(t)$ of the stochastic (full line) and CML (dashed line) models described in the caption of Fig. 3 plotted versus the square root of time. See the text for the definition of $w(t)$.

there is a reasonable agreement with the CML data. In particular, it can be seen that the average height u^* is definitely smaller than 1 in both cases: the reason can be traced back to the combined effect of the contraction mechanism with the diffusive process. Somehow larger differences can be observed in the behaviour of the variance $\sigma_u^2 = \langle (u_i(t))^2 \rangle - \langle u_i(t) \rangle^2$ but they can be attributed more to the approximation in the description of the perturbed region, rather than to peculiarities of the propagation.

In fact, if we look at the width $w(t)$ of the average front, defined as the distance between the rightmost sites where $\langle u_i(t) \rangle$ is larger than $0.8u^*$ and, respectively, $0.2u^*$, we observe a nearly square-root growth in both the CML and the stochastic model (see Fig. 4, where a nearly quantitative agreement is also observed). Moreover, we have verified that, keeping the contraction parameter a fixed, and increasing Δ up to small values (e.g. $\Delta \sim 0.01$), v_F slightly increases in both models.

On the basis of the results reported in Fig. 4, one can summarize our observations of the front dynamics by effectively assuming a stepwise shape for the profile at any time and approximating its motion with a diffusive process with drift. More precisely, we can write

$$\langle u_i(t) \rangle \approx \frac{u^*}{\sqrt{2\pi Dt}} \int_0^{+\infty} \Theta[x - (i - v_F t)] \exp\left(-\frac{x^2}{2Dt}\right) dx =$$

$$= \frac{u^*}{2} \left[1 - \operatorname{erf} \left(\frac{i - v_F t}{\sqrt{2Dt}} \right) \right], \quad (9)$$

where v_F is the average front velocity, while D is the “diffusion” coefficient accounting for the square-root growth in time for the standard deviation of the front position x (assumed to be continuous, for the sake of simplicity).

2.2 Further simplifications of the stochastic models

As we have verified that the qualitative features of the front dynamics do not depend on the shape of the probability distribution of $r_i(\tilde{u}_i, t)$, we have decided to simplify the stochastic models by assuming a δ -like distribution, i.e. that $r_i(\tilde{u}_i, t) = 1$. Moreover, in order to get rid of unnecessary technical complications we shall assume that $b = a$. Notice also that, having chosen $r_i(\tilde{u}_i, t) = 1$, we are obliged to assume $b < 1$, in order to avoid the appearance of a fictitious fixed point $u^* = 1$. From now on we study the following model

$$\begin{aligned} \tilde{u}_i(t) &= (1 - \varepsilon)u_i(t) + \frac{\varepsilon}{2}u_{i+1}(t) + \frac{\varepsilon}{2}u_{i-1}(t), \\ u_i(t+1) &= \begin{cases} 1, & \text{w.p. } p = a\tilde{u}_i(t) \\ a\tilde{u}_i(t), & \text{w.p. } 1 - p \end{cases}, \quad \text{if } \tilde{u}_i(t) > \Delta, \\ u_i(t+1) &= \begin{cases} \tilde{u}_i(t)/\Delta, & \text{w.p. } p = a\Delta \\ a\tilde{u}_i(t), & \text{w.p. } 1 - p \end{cases} \quad \text{if } \tilde{u}_i(t) \leq \Delta, \end{aligned} \quad (10)$$

that we call *Continuous Stochastic Model* (CSM). In the limit $\Delta \rightarrow 0$ it will be named *Discontinuous Stochastic Model* (DSM).

The only parameter that we are going to consider in the following sections is the contraction parameter a : this is sufficient to identify and characterize the relevant transition from the chaotic/unsynchronized phase to the ordered/synchronized one.

3 The zero dimensional case

The most important problem of linearly stable chaos is to understand how finite perturbations can propagate in spite of the average local contraction. To clarify this point, in this section we consider the zero-coupling limit, i.e. the 0-dimensional case. We shall see that even if “chaotic” motion cannot be sustained whenever the Lyapunov exponent is negative, the lack of a uniform contraction induces anyhow non-trivial properties.

Our first observation concerns the probability $P(t, u(0))$ for a finite-amplitude perturbation $u(0)$ to be never amplified by the instability mechanism over a time t . In the DSM, such a probability can be easily factorized as

$$P(t, u(0)) = \prod_{n=1}^t (1 - u(0)a^n) = \exp \left[\sum_{n=1}^t \ln(1 - u(0)a^n) \right] =$$

$$\begin{aligned}
&= \exp \left[- \sum_{k=1}^{\infty} \frac{u(0)^k}{k} \sum_{n=1}^t a^n \right] = \exp \left[- \sum_{k=1}^{\infty} \frac{u(0)^k}{k} \frac{a^k(1-a^{kt})}{1-a^k} \right] \\
&\xrightarrow{t \rightarrow \infty} \exp \left[- \sum_{k=1}^{\infty} \frac{(u(0)a)^k}{k(1-a^k)} \right] := \tilde{P}(u(0)) \quad . \quad (11)
\end{aligned}$$

One can see that, for $t \rightarrow \infty$, $P(t, u(0))$ approaches a finite value $\tilde{P}(u(0))$ that is both strictly larger than 0 and smaller than 1 for any value of $u(0)$ (if $0 < a < 1$). The same conclusion can be drawn also for the CSM, although the algebra is more complicate in that case. The inequality $\tilde{P}(u(0)) > 0$ indicates that the occasional amplifications are not so strong as to prevent the eventual absorption of the perturbation (this is consistent with our goal to deal with linearly stable processes). On the other hand, the inequality $\tilde{P}(u(0)) < 1$ indicates that the amplification process cannot be neglected. Notice that, since this holds true independently of $u(0)$ (although $\tilde{P}(u(0)) \rightarrow 1$ for $u(0) \rightarrow 0$), there is a difference with the convergence to a stable fixed point in a topologically chaotic map (think, e.g., of the logistic map in one of the stability windows that follow the first period doubling) since, in that case, there would be a threshold (corresponding to the border of the basin of attraction), below which a monotonous contraction would start. A closer similarity exists with the so-called strange nonchaotic attractors, as they are characterized by a nonmonotonous contraction even arbitrarily close to the attractor [21, 22].

The multifractal theory [23] provides the most appropriate framework to characterize this system. By following this approach, devised with reference to infinitesimal perturbations, we introduce the exponential growth rate of a finite initial perturbation $u(0)$,

$$\Lambda(t, u(0)) = \frac{1}{t} \ln \left(\frac{u(t)}{u(0)} \right). \quad (12)$$

In the limit $u(0) \rightarrow 0$, $\Lambda(t, u(0)) \rightarrow \lambda(t)$, the equivalent in this context of the usual finite-time Lyapunov exponent [24]. The proper indicator to look at is the probability distribution $\mathcal{P}(\Lambda, t, u(0))$ to find a growth rate between λ and $\Lambda + d\Lambda$ at time t starting from $u(0)$. More precisely, we introduce the finite-size multifractal spectrum

$$H(\Lambda) = \lim_{t \rightarrow \infty} \left[\frac{1}{t} \ln \mathcal{P}(\Lambda, t, u(0)) \right]. \quad (13)$$

As it will become clear later, $H(\Lambda)$ is independent of $u(0)$ (as long as $u(0) > 0$). Nevertheless, we shall show that it differs from the standard multifractal spectrum $h(\lambda)$, obtained by taking the limit $u(0) \rightarrow 0$ before the infinite-time limit

$$h(\lambda) = \lim_{t \rightarrow \infty} \lim_{u(0) \rightarrow 0} \left[\frac{1}{t} \ln \mathcal{P}(\Lambda, t, u(0)) \right]. \quad (14)$$

In other words, the order of the two limits is crucial for understanding the difference between the behaviour of infinitesimal and finite perturbations. In the following, we shall compare the multifractal distribution of $\lambda(t)$ (*linear analysis*) with that of $\lambda(t, u(0))$ (*nonlinear analysis*) in both stochastic models.

3.1 Linear analysis

We start from the CSM, as the DSM is nothing but a limit case of the former one. The linear approximation amounts to assuming $u_i(t) < \Delta \quad \forall i, t$. In this case, standard combinatorial analysis implies

$$h_{\Delta}(\lambda) = \frac{\ln(\Delta) + \lambda}{\ln(a\Delta)} \left[\ln(1 - a\Delta) - \ln \left(\frac{\ln(\Delta) + \lambda}{\ln(a\Delta)} \right) \right] + \frac{\ln(a) - \lambda}{\ln(a\Delta)} \ln \left[\frac{a\Delta \ln(a\Delta)}{\ln(a) - \lambda} \right], \quad (15)$$

where we have made explicit the dependence on the parameter Δ . In the limit $\Delta \rightarrow 0$, the above expression reduces to

$$h_0(\lambda) = \lim_{t \rightarrow \infty} \frac{1}{t} \ln \mathcal{P}[\lambda(t)] \xrightarrow{\Delta \rightarrow 0} \ln(a) - \lambda, \quad \lambda > \ln a \quad . \quad (16)$$

On the other hand, performing the limit $\Delta \rightarrow 0$ before the $t \rightarrow \infty$ limit would yield the trivial result $h_0(\lambda) = 0$ with the support of h_0 restricted to the point $\lambda = \ln a$. Thus, the non-commutativity of the limits $\Delta \rightarrow 0$ and $t \rightarrow \infty$ reveals that the discontinuous case is a singular limit of the CSM. In other words, the multifractal spectrum of the discontinuous model depends on the way it is defined. We prefer to adopt a “physical” point of view, i.e. to consider the discontinuity as the limit of a negligible Δ , which corresponds to taking first the $t \rightarrow \infty$ limit.

3.2 Nonlinear analysis

We now consider a finite perturbation $u(0)$ in the simple context $\Delta = 0$. From Eq. (12) we see that Λ is uniquely determined from the knowledge of $u(t)$ and $u(0)$ (and, obviously, the time t). Accordingly, the knowledge of $\mathcal{P}(\Lambda, t, u(0))$ is fully equivalent to that of the single-site probability distribution $Q(t, u)$, together with the initial condition

$$Q(0, u) = \delta(u - u(0)) \quad . \quad (17)$$

It proves useful to introduce the notation $u = a^n$ and $u(0) = a^{n_0}$, where n and n_0 are real variables ≥ 0 . Eq. (12) can be rewritten as

$$\lambda = \lambda(t, n, n_0) = \frac{1}{t} \ln \left(\frac{a^n}{a^{n_0}} \right) = \frac{n - n_0}{t} \ln a \quad . \quad (18)$$

Once $Q(t, n)$ is known, Eq. (18) allows one reconstructing the corresponding probability distribution $\mathcal{P}(\Lambda, t, u(0))$. Two possibilities are in order, either the system has never been “kicked”, i.e. reset to 1 by the instability mechanism, in which case the initial value has been contracted t -times by a factor a , or it has received at least one kick, losing memory of the initial condition. In the former case, occurring with probability $P(t, u(0))$, $\Lambda(t, u(0)) = \ln a$ or, equivalently, $n = n_0 + t$. In the latter case, $\Lambda(t, u(0)) > \ln a$ and the accessible values of n are restricted to positive integer numbers strictly smaller than $n_0 + t$ (since that the maximum possible contraction factor in t time steps is a^t). Accordingly, n can be interpreted as the elapsed time since the last kick, and the probability distribution $Q(t, u)$ can be factorized as the product of the probability $G(t - n, n_0)$ of receiving a kick at time $t - n$ for an initial perturbation $u(0) = a^{n_0}$ by the probability $P(n, 1)$ of not being kicked anymore for the remaining n time steps,

$$Q(t, n) = G(t - n, n_0)P(n, 1) \quad (19)$$

(in the remaining part of this section and in App. A, with no ambiguity arising, we denote with Q also the probability density of the logarithmic variable n). Moreover, we impose the condition $P(0, u(0)) := 1$ to extend the validity of Eq. (19) to the case $n = 0$.

The probability $G(t, n_0)$ can be recursively expressed as the probability of receiving the very first kick at time t plus the probability of receiving the second last kick at any previous time, i.e.

$$G(t, n_0) = a^{t+n_0} \prod_{k=1}^{t-1} (1 - a^{k+n_0}) + \sum_{k=1}^{t-1} G(k, n_0) a^{t-k} P(t - 1 - k, 1), \quad (20)$$

with $G(1, n_0) := a^{n_0+1}$. Eq. (20) can be numerically iterated in the large time limit to obtain the expression of the multifractal distribution (13). The analysis performed in App. A shows that $H(\Lambda)$, defined as in (13), is a segment of straight line restricted to the open interval $(\ln a, 0)$ of negative values. The slope of this straight line depends on the contraction parameter a but is independent of $u(0)$. In fact, in the appendix we show that the slope can be obtained by solving an eigenvalue problem, where $u(0)$ enters to specify the initial condition but not the operator itself. An approximate analytic solution is also determined, which confirms the numerical observation that the slope increases monotonously from -1 (for $a \rightarrow 0$) to 0 (for $a \rightarrow 1$). Curves 2 and 4 in Fig. 5 correspond to the nonlinear and linear analysis of the discontinuous case for $a = 0.7$, respectively. The latter curve lies well below the former one, indicating that the linear analysis leads to an underestimation of the fluctuations. This is a general fact holding for all values of a in the meaningful range $[0, 1]$. The difference must be attributed to the sporadic amplifications due to the discontinuity: it is remarkable that the finite-size spectrum is independent of the initial condition.

It is now important to test whether the difference between linear and non-linear curves persists also when the discontinuity is removed, i.e. in the CSM.

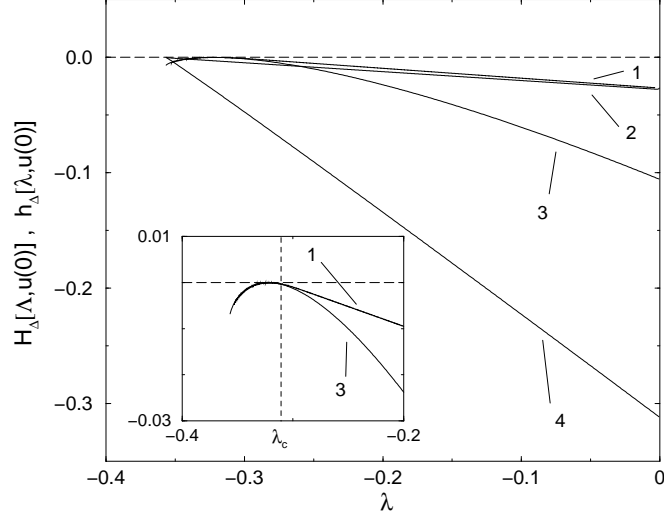


Figure 5: Probability distributions of the exponential growth rate (12) in the large time limit for the stochastic model (10) in the 0-dimensional case, with $a = 0.7$. Lines 1 and 3 refer to the continuous case ($\Delta = 0.0097$), with a finite size or an infinitesimal initial perturbation, respectively, while lines 2 and 4 refer to the discontinuous case ($\Delta \rightarrow 0$), still with a finite size or infinitesimal initial perturbation, respectively. Deviation from straight line of curve 2 is due to finite time effects. In the inset the difference between curves 1 and 3 is magnified.

For the sake of simplicity, we fix Δ equal to $a^{\bar{n}}$ and suppose that both \bar{n} and n_0 are non-negative integers, so that $u(t)$ is defined on a discrete subset of the unit interval, $\{a^n\}_{n=0,1,\dots}$. This assumption does not affect the main conclusions while it allows one writing a simple recursive equation for the probability distribution $Q(t, n)$:

$$\begin{aligned}
 Q(t+1, 0) &= \sum_{k=0}^{\bar{n}} Q(t, k) a^{k+1}, \\
 Q(t+1, n) &= \begin{cases} (1 - a^n) Q(t, n-1) + a^{\bar{n}+1} Q(t, n+\bar{n}) & 0 < n \leq \bar{n} \\ (1 - a^{\bar{n}+1}) Q(t, n-1) + a^{\bar{n}+1} Q(t, n+\bar{n}) & n > \bar{n} \end{cases} \quad (21)
 \end{aligned}$$

Equations (21), with the initial conditions $Q(0, n) = \delta_{n, n_0}$ and boundary conditions $Q(t, n) = 0 \forall t > n + n_0$, can be numerically iterated to obtain the finite-size multifractal distribution in the continuous case.

Since the development of analytical techniques to determine H_Δ is by far more complex than in the previous case, we have limited ourselves to determine the multifractal spectrum numerically. The linear and nonlinear spectra are reported in Fig. 5 for $\Delta = 0.0097$ (curves 3 and 1, respectively). Let us first

notice that the finite-size spectrum is again independent of the initial condition $u(0)$ and this makes H_Δ a well defined quantity: the effect of $u(0)$ is just to affect the convergence to the asymptotic spectrum. Furthermore, we can see that the nonlinear curve lies well above the standard multifractal spectrum, indicating that it is not the discontinuity to be responsible for the difference between the behaviour of infinitesimal and finite-size perturbations. Moreover, the overall closeness of curves 1 and 2 reveals that the removal of the discontinuity does not introduce significant differences in the finite-size spectrum.

Finally, let us closely compare $H_\Delta(\Lambda)$ with $h_\Delta(\lambda)$: the inset in Fig. 5 reveals that the two coincide for $\Lambda, \lambda < \lambda_c$ (see the dashed line), while above some critical value λ_c the finite-size spectrum continues as a straight line, while h_Δ decreases faster. In the language of thermodynamic formalism, the linear behaviour of H_Δ is suggestive of a phase transition, from small values of Λ , that are correctly described by the linear analysis, to large values of Λ , where the finite character of the perturbation cannot be neglected. This point would certainly require a more detailed analysis to provide a more solid background to the above arguments, but we avoid this as it would drive us too far from what is the main goal of the present paper.

The analysis performed in this section has allowed us introducing well defined observables to deal with finite-size perturbations. We cannot, however, avoid commenting on an alternative class of tools that have been devised to deal with this problem, although mainly in the context of truly chaotic systems. Since in realistic physical conditions perturbations are always finite, it is very tempting to introduce a growth rate to characterize perturbations of different sizes. However, serious conceptual problems are immediately encountered if one tries to define truly finite-size Lyapunov exponents. On the one hand, the finiteness of the size induces a dependence on the norm utilized, on the other hand it requires that the Lyapunov exponent has to be defined for a finite-time resolution, since perturbations change size over time. This latter implication is rather crucial in that so defined Lyapunov exponents are not self-averaging quantities (see Ref. [16] for a detailed discussion of the problem).

In spite of such limitations, finite-size Lyapunov exponents may carry useful information, although one has to be careful in interpreting them. Let us, for instance, look at

$$\Lambda_0(u) = \left\langle \ln \frac{u'}{u} \right\rangle \quad (22)$$

where u' is the first iterate of u in the DSM and the average is performed over all possible realizations of the stochastic process. Simple algebra yields

$$\Lambda_0(u) = \ln a - au \ln(au) \quad . \quad (23)$$

In the limit $u \rightarrow 0$, $\Lambda_0(u)$ reduces correctly to the true Lyapunov exponent $\log a$. If a is not too small ($a > 1/e$, where e is the Neper number), $\Lambda_0(u)$ has a maximum value for an intermediate value of u and, more interestingly, the maximum

value of Λ is larger than 0, if $a > \exp(-1/e) = 0.692\dots$. Therefore, this result is suggestive of a phase transition from a regime (small a) where perturbations of all sizes decrease, to a regime where sufficiently large perturbations expand (and can, in principle, self-sustain). However, we already know that this conclusion is incorrect: the reason is precisely that $\Lambda_0(u)$ is an average quantity, and fluctuations must be taken into account. In fact, a different scenario arises, if we define the contraction rate by taking the logarithm of the average expansion factor. In this case, we obtain

$$\Lambda_1(u) = \ln a + \ln(2 - au), \quad (24)$$

an expression that can be larger than zero even at $u = 0$, where it actually attains its maximum value! In practice, one has to be very careful in drawing meaningful conclusions from any expression of the finite-size Lyapunov exponent. In particular, since u can never be larger than 1, while it can become arbitrarily small, the typical negative contraction rate operating at small u -values eventually wins, making always $u = 0$ the only stable fixed point.

4 The spatially extended case

The past study of stable chaos has revealed that no qualitative difference exists, as long as strictly finite chains are considered, with respect to standard stable systems. After an exponentially long transient, a periodic behaviour is always attained. As it was remarked in Section II, a similar scenario is indeed exhibited by our stochastic models.

Eq. (11) shows that in the absence of any coupling, there is a finite probability $\tilde{P}(u(0))$ for an initial perturbation $u(0)$ to be contracted for an infinite amount of time steps and thus of being effectively absorbed. It is worth defining here

$$u_M(t) = \max_i u_i(t) \quad . \quad (25)$$

In particular, this allows us applying the above reasoning to the coupled case, with $u_M(0)$ playing the role of $u(0)$; the probability \tilde{P} that an arbitrary, spatially extended, perturbation is contracted forever on every site i satisfies the inequality

$$\tilde{P}(\{u_i\}_{i=1,\dots,L} \geq \left[\prod_{n=1}^{\infty} (1 - u_M(0)a^n) \right]^L = \left[\tilde{P}(u_M(0)) \right]^L \quad , \quad (26)$$

where $\tilde{P}(u_M(0))^L$ is small but finite for every finite lattice length L . Thus, the average time τ needed for any perturbation to die out (i.e. to be contracted below some arbitrarily small threshold value) is finite and does not grow faster than exponentially with the system size,

$$\tau \leq \left[\tilde{P}(u_M(0)) \right]^{-L} \quad . \quad (27)$$

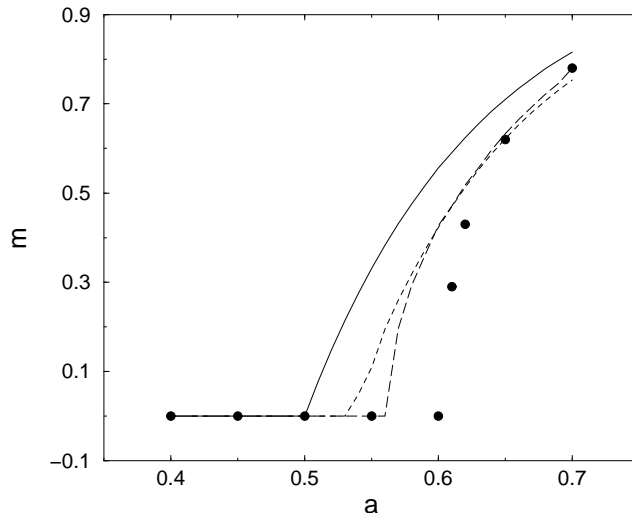


Figure 6: The space-time and ensemble average value \tilde{m} of the perturbation $u_i(t)$ as a function of the contraction rate a . The dots refer to the result of numerical simulations with lattices of size $L = 1000$; the solid, dashed, and long-dashed curves refer to the mean field analysis, the Gaussian approximation discussed in the appendix B, and the numerical integration of the Frobenius-Perron equation (29), respectively.

In the active, i.e. chaotic, phase where perturbations propagate with a finite velocity, τ grows exactly exponentially (with the system size), since the only way for a perturbation to die out is to be contracted in all sites, while in the inactive phase, the latter is only a sufficient condition and not a necessary one, and perturbations die out on significantly shorter time scales.

At variance with the 0-dimensional case, direct numerical simulations of the DSM in a 1-d lattice reveal the existence of a regime where finite perturbations self-sustain. This is clearly shown in Fig. 6, where we have reported the space-time and ensemble average value \tilde{m} of the perturbation for different values of the contraction rate. Above $a = 0.60(5)$, nonzero amplitudes are actually observed. It is, therefore, crucial to understand the reason why the spatial interactions can stabilize finite perturbations in spite of the diffusive nature of the coupling.

The natural extension of what we have learnt in zero-dimension consists in looking at the joint probability distribution $R(t, u_1, u_2, \dots, u_n, \dots)$ over the whole lattice. If the system is sufficiently above the transition to stable chaos, it seems reasonable, in a first approximation, to neglect spatial correlations. This is certainly incorrect for those sites that are close to propagating fronts but the fraction of such lattice sites is definitely negligible. Accordingly, we approximate

the joint probability distribution as a product of single-site probabilities $Q(t, u)$,

$$R(t, u_1, u_2, \dots, u_n, \dots) \approx Q(t, u_1)Q(t, u_2) \dots Q(t, u_n) \dots \quad (28)$$

Within this approximation, the single-site probability distribution corresponding to the stochastic dynamics (10) satisfies the following Frobenius-Perron equation,

$$\begin{aligned} Q(t+1, u) &= g(u) \int_0^\infty \prod_{i=1}^N dv_i Q(t, v_i) \delta \left(u - \frac{a}{N} \sum_{i=1}^N v_i \right) \\ &\quad + a\Delta \int_0^\infty \prod_{i=1}^N dv_i Q(t, v_i) \delta \left(u - \frac{1}{N\Delta} \sum_{i=1}^N v_i \right) \\ Q(t+1, 1) &= \int_{a\Delta}^\infty du u \int_0^\infty \prod_{i=1}^N dv_i Q(t, v_i) \delta \left(u - \frac{a}{N} \sum_{i=1}^N v_i \right), \end{aligned} \quad (29)$$

where δ is the Dirac's distribution, v_i is the amplitude of the perturbation in the i th neighbouring site, N is the number of democratically coupled sites (for later convenience we leave N unspecified - notice that $N = 3$ in a 1-d lattice with nearest-neighbour coupling) and

$$g(u) = \begin{cases} 1 - u & \Delta < u < 1 \\ 1 - a\Delta & 0 \leq u \leq \Delta \end{cases}.$$

It is easy to verify that the support of the single-site probability distribution $Q(t, u)$ remains confined to the unit interval, provided that this holds true for the initial condition as well. Furthermore, due to the factorization hypothesis, the space and ensemble average $m(t)$ defined in Section II coincides with the simplest ensemble average, i.e. the mean value of $Q(t, u)$.

In Fig. 7 we have plotted the single site probability distributions obtained by directly iterating the stochastic model and the approximate Frobenius-Perron equation (29) (solid and dashed line, respectively). The reasonable overlap confirms the validity of the factorization hypothesis (at least away from the critical region). The mean value, equal to 0.773 in former case, compares with 0.770 in the latter one, while the variances are respectively equal to 0.063 and 0.061. Such small differences are due to the different behavior of the probability distributions for small values of u .

For $N = 1$ (no coupling), Eq. (29) corresponds to the 0-dimensional dynamics discussed in the previous section, and the evolution equation is exact. It reduces to the linear equation,

$$\begin{aligned} Q(t+1, u) &= g(u) \frac{1}{a} Q(t, \frac{1}{a}u) + a\Delta^2 Q(t, a\Delta u) \\ Q(t+1, 1) &= a \int_{\Delta}^\infty du u Q(t, u), \end{aligned} \quad (30)$$

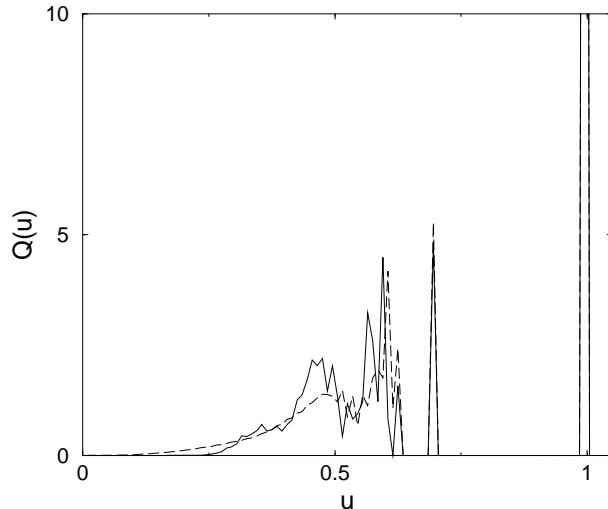


Figure 7: Stationary, single-site probability distribution $\tilde{Q}(u)$ for $a = 0.7$ and $\Delta = 0.01$ computed by numerical simulation of the CSM (dashed line) and by numerical solution of Eq. (29) for $N = 3$ (solid line). Both distributions have been obtained subdividing the unit interval in 100 channels. The δ -peak in $u = 1$ has been cut to magnify all other details.

The only fixed point of this equation is $Q(t, u) = \delta(u)$, i.e. the absorbing state. The multifractal spectrum discussed in Sec. III is nothing but a sophisticated characterization of the convergence towards such a fixed point.

On the opposite side of the 0-dimensional limit, there is the mean-field approximation that corresponds to the limit $N \rightarrow \infty$. In this limit, statistical fluctuations vanish and the dynamics reduces to the evolution of the mean value $m(t)$, that reads

$$m(t+1) = \begin{cases} m(t)[2a - a^2m(t)] & \text{if } m(t) > \Delta \\ m(t)[2a - a^2\Delta] & \text{if } m(t) \leq \Delta. \end{cases} \quad (31)$$

For $a < a_c = (1 - \sqrt{1 - \Delta})/\Delta$, Eq. (31) displays the stable fixed point $m_1 = 0$. This is the same regime found in 0-dimension and corresponds to the eventual absorption of any initial finite difference. Increasing a above a_c , the system undergoes a bifurcation: m_1 becomes unstable and a second (stable) fixed point $m_2 = (2a - 1)/a^2$ appears. In the discontinuous limit ($\Delta \rightarrow 0$) $a_c \rightarrow 1/2$. In Fig. 6 the predictions of the mean-field approach are compared with the results of direct simulations: we see that, in spite of the approximations, there are no severe differences and the critical point is underestimated by approximately 17%.

It is rather instructive to notice that the predictions of the mean-field analysis do coincide with the finite-size Lyapunov exponent Λ_1 (for the sake of simplicity, we limit ourselves to consider the DSM). Since the mean field approximation reduces the CSM dynamics to the evolution of a single variable $m(t)$, the comparison can be performed by interpreting $\ln[m(t+1)/m(t)]$ as Λ_1 and recalling that Eq. (24) has been derived for the DSM only. Even though Eq. (24) can be obtained by Eq. (31), there is an important difference between the consequences of the two results. As we discussed in Section III, fluctuations keep $u^* = 0$ stable for every value of a , while in the case of the mean field analysis, the lack of any fluctuation, due to the formally infinite number N of neighbours, implies that the fixed point $u = 0$ is truly unstable when $a > 1/2$.

The absence of fluctuations in the mean field limit implies that all definitions of the finite-size Lyapunov exponent are equivalent. Therefore, we observe the same scenario previously observed for the standard maximum Lyapunov exponent: the diffusive coupling shifts the Lyapunov exponent from the average value of the logarithm of the multiplier (the so-called quenched average holding for the single map) towards the logarithm of the average multiplier (annealed average, predicted by the mean field analysis). The important consequence of this shift is that, in the present context, it can change the stability of the $u = 0$ solution leading to the onset of the chaotic phase.

Anyway, one should not forget that the mean-field analysis provides an approximate solution. For N finite and strictly larger than 1, Eq. (29) defines a non trivial evolution operator \mathcal{Q} in a functional space. In practice, one can expand the evolution equation into an infinite set of equations for, e.g. the momenta M_k of Q . An approximate solution can thus be found by either suitably truncating the hierarchy of equations or introducing a closure Ansatz. In App. B we parametrize the probability distribution as the sum of a δ -distribution and a Gaussian. This allows us deriving three evolution equations for the DSM.

In both cases that we have investigated ($N = 2, 3$), we find a scenario similar to the one predicted by the mean field analysis. There exists a critical value a_c (equal to 0.548 for $N = 2$ and to 0.536 for $N = 3$) below which the dynamics is characterized by the stable fixed point $A = 1, v = 0, V = 0$ (corresponding to the absorbing state $Q(t, v) = \delta(v)$) and above which the previous solution becomes unstable, giving rise to a stable nontrivial solution. The dependence of m on a reported in Fig. 6 (see the dashed curve in Fig. 6) indicates that the critical value predicted by this analytic approach improves the mean-field estimate, but the growth of m above threshold is not as good as one would like. In fact, there is a qualitative difference with the mean-field approach: a further bifurcation (at $a = \bar{a} = 0.855$ for $N = 2$ and $\bar{a} = 0.869$ for $N = 3$), where the new solution destabilizes too. Such a bifurcation and the slow growth of \tilde{m} with a are both consequences of a defect of the approximation: the support of the Gaussian extends out of the unit interval. This unphysical property becomes increasingly important as soon as the average amplitude of u is comparable with 1.

Indeed, a better agreement with the direct simulations is obtained by iterating numerically the Frobenius-Perron equation (see Fig. 6). Neither simulations performed with $\Delta = 0$ nor with $\Delta = 0.01$ reveal the second bifurcation found with the Gaussian approximation, confirming that it is an artifact of the approximation. In the continuous case, the bifurcation occurs at the critical value $a_c = 0.591\dots$ (for $N = 2$) and $a_c = 0.568\dots$ (for $N = 3$), to be compared with the mean field prediction $a_c = 0.501\dots$. In the discontinuous case we find $a_c = 0.585\dots$ (for $N = 2$) and $a_c = 0.567\dots$ (for $N = 3$), to be compared with the mean field prediction $a_c = 0.5$.

From the data reported in Fig. 6 for $N = 3$ we see that the factorization hypothesis reproduces fairly well the behaviour of the full stochastic model everywhere except for the transition region. This is not unexpected as it is well known that the correlation length diverges in the critical region.

5 Open problems and conclusions

In this paper we have shown that a simple *stochastic* model, specifically designed to simulate a different response to finite and infinitesimal perturbations, is able to capture the key features of irregular behaviour in linearly stable systems. In particular, we have seen that replacing the sequence of jumps generated by the CML dynamics with a genuine stochastic process allows for a faithful reconstruction of the front propagation. The main theoretical advantage of the stochastic model is the disentanglement between the generation of a pseudo-random pattern and the evolution of perturbations. In reality the two issues are interlaced: their separation has allowed us clarifying under which conditions (finite) perturbations can be effectively sustained throughout an infinite lattice. In particular, a full consistency exists between the CML and the stochastic model in the chaotic regime, since we can state that the amplification of finite perturbations contributes to sustain an irregular regime.

On the other hand, the transition to the ordered phase observed in the CSM/DSM models does not reproduce the analogous behaviour displayed by the CML. In this latter case, it was observed that the critical region is not point-like, but rather extended to a what has been called “fuzzy region”, where ordered and chaotic dynamics alternate in a quite irregular manner [17]. The reason for the difference is that in the CML model, the absence of local chaos makes the sequence of multipliers increasingly less random in the transition region. In the stochastic model, instead, the randomness of multipliers is always assumed a priori. In spite of such a difference, it is nevertheless instructive to notice that a transition persists without modifying the stochasticity in the real space.

A more precise analogy for the transition investigated in the previous section is provided by the correspondence with the problem of synchronization in the presence of external noise. In fact, in this latter context, the noise represents the (unavoidable) source of stochasticity in the synchronous as well as in the

asynchronous regime. Since a recent numerical study of the synchronization transition in linearly stable system has suggested that it belongs to the universality class of Directed Percolation (DP) [18], it is tempting to verify whether the same holds true in our stochastic models.

As already mentioned, even though the front velocity v_F is a good order parameter to characterize the transition, it is quite difficult to obtain a reliable estimate of the critical value of the control parameter a_c from the vanishing of v_F . In fact, finite-size and transient effects combined with the existence of wild fluctuations prevent a careful analysis. A more efficient method amounts to measuring the dependence of the so-called *absorption time* τ on the system size L . This is defined as the time required for the space averaged perturbation $\bar{u}(t)$ to become smaller than some very small, but finite threshold Γ . Fluctuations of τ can be efficiently reduced by averaging over a sufficiently large ensemble of initial conditions. In the active phase, τ is expected to diverge exponentially with L (stable chaotic regime), while in the absorbing phase, it should depend at most logarithmically on L . Only at the critical point, τ exhibits a power law dependence

$$\tau(L, a_c) \sim L^z, \quad (32)$$

where $z = \nu_l/\nu_\perp$ is the so called dynamical exponent. We have performed numerical simulations for both the CSM (with $\Delta = 0.01$) and DSM, averaging over 3000 realizations of the stochastic process and over randomly sampled initial conditions. In the CSM we find $a_c = 0.6055\dots$, with $z = 1.58 \pm 0.02$; in the DSM we obtain $a_c = 0.6065\dots$ and $z = 1.56 \pm 0.06$. The errors have been estimated as the maximum deviation from linearity in the log-log plot that has been used for extracting the scaling law (32) (see, for instance, Fig. 8, where τ has been plotted versus L for $\Delta = 0.01$ and different values of a). These results agree with the most accurate numerical estimates of the DP value, $z = 1.5807$ [25].

We also measured the critical exponent δ associated with the temporal decay of the density of active sites $\rho(t)$, i.e. those sites where $u_i(t) > \Gamma$: at the critical point $\rho(t)$ is characterized by the scaling law

$$\rho(t, a_c) \sim t^{-\delta}, \quad (33)$$

where $\delta = \beta/\nu_l$ (as usual ν_l , ν_\perp and β are the critical exponents respectively associated with space and time correlation lengths and with the order parameter). By averaging over 3000 realizations and choosing a sufficiently large value of L to get rid of finite-size corrections we have found $\delta = 0.150 \pm 0.01$ for the CSM and 0.155 ± 0.005 for the DSM, to be compared with the DP value $\delta = 0.1595$ [25].

Altogether, our simulations support the hypothesis that the transition belongs to the same universality class as DP. This may look as an almost trivial result, since local spreading is the only mechanism for the propagation of perturbations (or, in different languages, active sites, infections). However, the

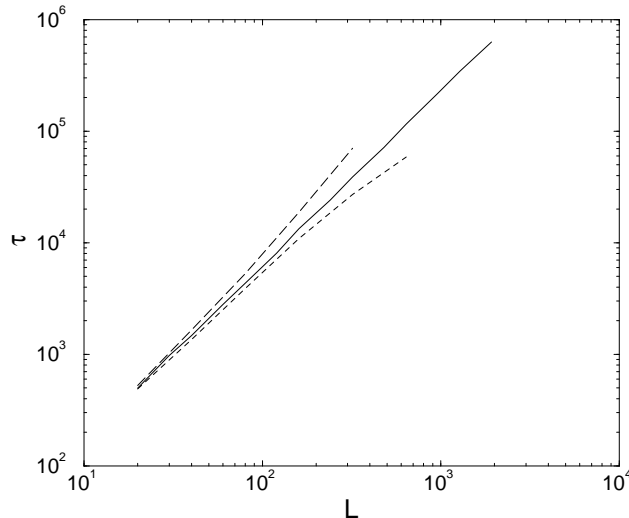


Figure 8: Log-log plot of the absorption time τ as function of the system size L in the continuous case ($\Delta = 0.01$) near the critical value for different control parameter values: $a = 0.6051$ (dashed line), $a = 0.655$ (solid line), and $a = 0.6061$ (long-dashed line).

whole problem is definitely more subtle, as an absorbing state cannot be identified so clearly. In fact, we have already seen that the determination of the absorption time requires to fix a somehow arbitrary threshold Γ , and the same is true for the computation of the active sites at a given time. Even though we have found that our results are independent of the choice of Γ (provided that it is small enough), this may appear as a numerical trick: there is nothing like a true threshold, since no matter how small is a perturbation, there is always some finite probability that it gives rise to a burst: this is contrary to the existence of a truly absorbing state. On the other hand, the argument presented in the beginning of the previous section to convince the reader that in a finite chain any perturbation eventually dies out, confirms the existence of an absorbing state: since the smaller is u_M the more likely is that the perturbation keeps being absorbed, any perturbation $u_i(t)$ has a finite probability to enter an infinite “contraction loop” in which every site i is monotonously contracted for any time larger than t .

It would be nice to put our qualitative arguments on a more rigorous basis, by defining a suitable finite-size Lyapunov exponent that is negative below some threshold to indicate that $u^* = 0$ is a truly absorbing state. However, it is not clear whether this could be accomplished, since we know that in the chaotic phase, $u^* = 0$ should be at the same time “macroscopically” unstable since perturbations eventually drive the system towards the only stable state

and “microscopically” stable to mean that small enough perturbations have to be absorbed. In the future, we hope to be able to clarify whether it is possible to define an indicator that contains both messages.

RL and AP wish to thank R. Kapral for early discussions about a meaningful definition of the stochastic model. A. Pikovsky, V. Ahlers and A. Torcini are acknowledged for useful exchanges of ideas about the characterization of the transition. A profitable discussion on the 0-dimensional model has been carried on with Y. Elskens. Part of this work has been completed thanks to the financial support of the NATO contract CRG.973054. We also thank I.S.I. in Torino where part of this work was performed.

A Multifractal distribution

In this appendix we report the analytical calculation of the (constant) slope of the multifractal distribution (13) for the zero dimensional DSM. We shall prove that $H'(\Lambda, u(0))$ (the prime denotes derivative with respect to Λ) is independent of Λ and increases monotonously with the contraction rate a from -1 (for $a \rightarrow 0$) to 0 (for $a \rightarrow 1$).

First of all, note that the condition $0 \leq n \leq n_0 + t$, together with Eq. (18), implies that the support of $H(\Lambda)$ is confined in the interval $[\ln a, 0]$, since the ratio $\rho = n/t$ can take values between 0 and 1 and in the $t \rightarrow \infty$ limit n_0/t vanishes.

We are now interested in the $\Lambda > \ln a$ case (i.e. the one in which the system received at least one kick), where, as it was stated in Section III, the actual size of the perturbation u at time t is unambiguously determined by the time $n < t$ elapsed since the last kick (see Eq. (18)) and thus, for any finite t , both u and Λ can assume only a discrete set of values labelled by n .

Let us now denote the discrete Λ -derivative of a generic function $f(\Lambda)$ as

$$D_\Lambda(f) = \frac{f(\Lambda + \Delta\Lambda) - f(\Lambda)}{\Delta\Lambda}. \quad (34)$$

From Eq. (13), we can approximate the derivative of the multifractal distribution H as

$$H'(\Lambda, u(0)) = \lim_{t \rightarrow \infty} \frac{D_\Lambda(\ln \mathcal{P}(\Lambda, t, u(0)))}{t}, \quad (35)$$

where $\Delta\Lambda$ is naturally fixed by Eq. (18) and the discrete character of $n = \ln u / \ln a$,

$$\Delta\Lambda = \Lambda_{\tau+1}(t, u(0)) - \Lambda_\tau(t, u(0)) = \frac{\ln a}{t}. \quad (36)$$

As, for $t \rightarrow \infty$, $\Delta\Lambda$ goes to 0, Eq. (35) becomes asymptotically exact.

Morover, Eq. (18) allows one switching to the Q representation of probabilities writing

$$H'(\Lambda, u(0)) = \frac{1}{\ln a} \lim_{t \rightarrow \infty} \ln \left[\frac{\mathcal{P}(\Lambda + \Delta\Lambda, t, u(0))}{\mathcal{P}(\Lambda, t, u(0))} \right] = \frac{1}{\ln a} \lim_{t \rightarrow \infty} \ln \left[\frac{Q(t, n+1)}{Q(t, n)} \right] \Big|_{n=n_0 + \frac{t\Lambda}{\ln a}} \quad (37)$$

(remember also that $u(0) = a^{n_0}$). Making use of Eqs. (19) and (11), we obtain

$$H'(\Lambda, u(0)) = \frac{1}{\ln a} \left[\ln \left(\frac{G(t-n-1, n_0)}{G(t-n, n_0)} \right) + \ln(1 - a^{n+1}) \right] \Big|_{n=n_0 + \frac{t\Lambda}{\ln a}}. \quad (38)$$

In the limit $t \rightarrow \infty$, the last term in the r.h.s. vanishes, provided n diverges too (i.e. $\Lambda < 0$). We are thus left with the following equality, which holds true for any Λ in the open interval $(\ln, 0)$,

$$H'(\Lambda, u(0)) = -\frac{\ln \eta(a, n_0)}{\ln a}, \quad (39)$$

where

$$\eta(a, n_0) = \lim_{t \rightarrow \infty} \frac{G(t+1, n_0)}{G(t, n_0)}, \quad (40)$$

the n -dependence has been eliminated by shifting the time origin and the dependence on the parameter a has been made explicit. From this equation, we see that the problem of determining the slope of the multifractal spectrum is equivalent to an eigenvalue problem. In fact, we can formally write Eq. (20) as

$$\vec{v}(t, n_0) = M\vec{v}(t-1, n_0), \quad (41)$$

where $\vec{v}(t, n_0)$ is the infinite-dimensional vector

$$\vec{v}(t, n_0) \equiv (G(t, n_0), G(t-1, n_0), G(t-2, n_0), \dots), \quad (42)$$

and M is a linear infinite-dimensional operator. Therefore, $\eta(a)$ is nothing but the maximum eigenvalue of the operator M .

From the explicit expression of the recursive equation for $G(t, n_0)$ (see Eq. (20))

$$G(t, n_0) = G(t-1, n_0)P(0, 1)a + G(t-2, n_0)P(1, 1)a^2 + \dots + a^{n_0} \prod_{k=1}^{t-1} (1 - a^{k+n_0})a^t, \quad (43)$$

we see that, since both $G(t, n_0)$ and $P(t, 1)$ are not larger than 1 (they are probabilities), the sum in the r.h.s. is bounded from above by the sum of the first t powers of a . In the limit $t \rightarrow \infty$, the function $G(t, n_0)$ converges exponentially fast, so that we are able to truncate Eq. (43) to order k with an arbitrary precision. This truncation makes the problem numerically solvable,

as the operator M can be approximated by the finite dimensional matrix M_k (here and below, the subscript k stands for k th order approximation) that we report here below,

$$M_k = \begin{pmatrix} \alpha_1 & \alpha_2 & \alpha_3 & \cdots & \alpha_k \\ 1 & 0 & 0 & \cdots & 0 \\ 0 & 1 & 0 & \cdots & 0 \\ 0 & 0 & 1 & \cdots & 0 \\ \vdots & \vdots & \vdots & \ddots & \vdots \\ 0 & 0 & 0 & \cdots & 1 \end{pmatrix}, \quad (44)$$

where $\alpha_j = a^j P(j-1, 1)$. Numerical estimates of $\eta_k(a)$ indicate that $k = 10$ suffices to attain a good convergence in the whole range of a values between 0 and 1. For $k = 2$ the eigenvalue $\eta_2(a)$ can be computed analytically yielding,

$$H_2'(\Lambda, u(0)) = -1 - \frac{1}{\ln a} \ln \frac{1 + \sqrt{5 - 4a}}{2}, \quad (45)$$

which goes monotonously from -1 ($a \rightarrow 0$) to 0^- ($a \rightarrow 1$).

B An approximate solution of the 1-dimensional problem

The Frobenius-Perron operator defined by Eq. (29) is a functional equation whose solution requires projecting it onto a finite dimensional space either via some truncation or a suitable closure hypothesis. Looking at a typical shape of the stationary probability distribution in Fig. 7, we can see that the multi-peaked structure slows down the convergence of an expansion in either moments or cumulants. Accordingly, we have preferred to approximate the probability distribution as the sum of a Dirac's δ distribution centered in 1 (the reinjection point) plus a Gaussian distribution, centered around a point to be determined self-consistently,

$$Q(t, v) = A_t \delta(v - 1) + \frac{1 - A_t}{\sqrt{2\pi V_t}} \exp \left[-\frac{(v - \bar{v}_t)^2}{2V_t} \right]. \quad (46)$$

We can see that $Q(t, v)$ is parametrized by three quantities: A_t , the probability of the δ component, V_t the variance of the Gaussian, and \bar{v}_t , its average value. The mean value $m(t)$ of $Q(t, u)$ is therefore equal to

$$m(t) = 1 - A_t + A_t \bar{v}_t. \quad (47)$$

It should be noted that our approximation is formally “unphysical” since the support of any Gaussian function is not restricted to the unit interval, but we

expect our Ansatz to be reasonably correct as long as the probability to be out of the unit interval is small enough.

Entering the above definition of $Q(t, v)$ into Eq. (29) and computing separately the new weight of the δ component, the average and the variance of the Gaussian, we obtain three evolution equations. In the simplest nontrivial case, $N = 2$, we have

$$\begin{aligned}
A_{t+1} &= a [A_t(1 - \bar{v}_t) + \bar{v}_t] \\
\bar{v}_{t+1} &= -v_t^2 [2 - A_t] \frac{a^2}{2} + \bar{v}_t a [1 - aA_t] - a \left[1 + \frac{a}{2}(V_t - 2 + A_t) - \frac{1 - a}{1 - A_t} \right] \\
V_{t+1} &= v_t^3 \left[-A_t \left(a - \frac{3}{4}a^2 \right) - (1 - a)^2 \right] a + \bar{v}_t^2 \left[A_t(2 - a) \frac{3}{4}a^2 + a^2 - a + \frac{1 - a}{1 - A_t} \right] + \\
&\quad \bar{v}_t \left[-A_t(1 - V_t) \frac{3}{4}a^3 - \frac{3}{2}a^3 V_t + a^2(V_t - 2) + 2a - \frac{2a(1 - a)}{1 - A_t} \right] - \\
&\quad A_t [a(V_t - 1) + 2] \frac{a^2}{4} + a^3 + \frac{a^2}{2}(V_t - 2) + \frac{a^2 - a^3}{1 - A_t}.
\end{aligned} \tag{48}$$

For $N = 3$, the case that we have investigated in detail as it corresponds to a 1-d lattice of democratically coupled maps, the equations read

$$\begin{aligned}
A_{t+1} &= a [A_t(1 - \bar{v}_t) + \bar{v}_t] \\
\bar{v}_{t+1} &= -\bar{v}_t^2 [3 - A_t] \frac{a^2}{3} + \bar{v}_t (a - \frac{4}{3}a^2 A_t) - a \left[1 + \frac{a}{3}(V_t - 3 - 2A_t) - \frac{1 - a}{1 - A_t} \right] \\
V_{t+1} &= \bar{v}_t^3 \left[-\frac{2}{9}A_t^2 a^2 + \frac{2}{9}A_t(5a - 2)a - (1 - a)^2 \right] a + \\
&\quad \bar{v}_t^2 \left[\frac{2}{3}A_t^2 a^3 - \frac{2}{3}A_t(2a - 3)a^2 + a^2 - a + \frac{1 - a}{1 - A_t} \right] - \\
&\quad \frac{2\bar{v}_t}{3} \left[A_t^2 a^3 - A_t(-3 + 2a + V_t a) - 2a \left(-a^2 - 1 + \frac{V_t}{2}(2 - 3a)a - 3 \frac{1 - a}{1 - A_t} \right) \right] + \\
&\quad A_t^2 \left(\frac{2}{9}a^3 + a^2 - a \right) - A_t \left[\frac{2}{3}a^3(V_t + \frac{4}{3}) - \frac{1}{3}a^2 + a \right] + \\
&\quad \frac{8}{9}a^3 + V_t \frac{a^2}{3} - a + \frac{2(a - a^3)}{1 - A_t}.
\end{aligned} \tag{49}$$

In spite of the great simplifications involved in the derivation of both sets of equations, it is still impossible to obtain an analytic expression even for the critical point a_c . The results of the numerical solution of Eq. (49) and (50) are discussed in the text (see Sec. IV).

References

- [1] J.-P. Eckmann and D. Ruelle, Rev. Mod. Phys. **67**, 617 (1985).

- [2] K. Kaneko, *Progr. Theor. Phys.* **74**, 1033 (1984).
- [3] R. Livi, A. Politi, and S. Ruffo, *J. Phys. A* **19**, 2033 (1986).
- [4] P. Grassberger, *Phys. Scr.*, **40**, 346 (1989).
- [5] S. Wolfram (ed.), *Theory and Applications of Cellular Automata*, World Scientific, Singapore (1986).
- [6] J. P. Crutchfield and K. Kaneko : *Phys. Rev. Lett.* **60**, 2715 (1988).
- [7] A. Politi, R. Livi, G.L. Oppo, and R. Kapral, *Europhys. Lett.* **22**, 571 (1993).
- [8] R. Livi, G. Martinez-Mekler, and S. Ruffo, *Physica D* **45** , 452 (1990).
- [9] R. Kapral, R. Livi, G.L. Oppo, and A. Politi : *Phys Rev* **E49**, 2009 (1994).
- [10] Y. Cuche, R. Livi, and A. Politi, *Physica D* **103**, 369 (1997).
- [11] R. Kapral, R. Livi, and A. Politi , *Phys. Rev. Lett.* **79**, 2277 (1997).
- [12] R. Livi, S. Ruffo, and A. Politi, *J. Phys A* **25**, 4813 (1992).
- [13] F. Cecconi and A. Politi, *J. Phys. A*, **32**, 7603 (1999).
- [14] G. Boffetta, M. Cencini, M. Falcioni, and A. Vulpiani, *nlin.CD/0101029*.
- [15] M. Cencini and A. Torcini, *nlin.CD/0011044*.
- [16] T. Letz and H. Kantz, *Phys. Rev. E* **61**, 2533 (2000).
- [17] F. Cecconi, R. Livi, and A. Politi, *Phys. Rev. E* **57**, 2703 (1998).
- [18] L. Baroni, R. Livi, and A. Torcini, *Phys. Rev. E*, in print.
- [19] E. Domany and W. Kinzel, *Phys. Rev. Lett.* **55**, 311 (1984). For a recent review see: P. Grassberger, *Directed Percolation: Results and Open problems*, in “Nonlinearities in Complex Systems”, Proceedings of 1995 Shimla Conference on Complex Systems, S. Puri et al eds. (Narosa Publishing, New Dehli 1997).
- [20] A. Politi and A. Torcini, *Europhys. Lett.* **28**, 545 (1994).
- [21] A. Pikovsky and U. Feudel, *CHAOS* **5**, 253 (1995)
- [22] U. Feudel, J. Kurths, and A. Pikovsky *Physica D*, **88**, 176 (1995).
- [23] C. Beck and F. Schlögl, *Thermodynamics of chaotic systems* (CUP, Cambridge 1993).
- [24] G. Paladin and A. Vulpiani, *Phys. Rep.* **156**, 147 (1987).
- [25] I. Jensen, *J. Phys. A* **29** 7013 (1996); *cond-mat/9906036/*.